https://doi.org/10.20965/jdr.2016.p0015

Paper:

Preliminary Results of Weather Radar Observations of Sakurajima Volcanic Smoke

Masayuki Maki[*1], **Masato Iguchi**[*2], **Takeshi Maesaka**[*3], **Takahiro Miwa**[*3], **Toshikazu Tanada**[*3], **Tomofumi Kozono**[*4], **Tatsuya Momotani**[*5], **Akihiko Yamaji**[*5], **and Ikuya Kakimoto**[*6]

[*1]Research and Education Center for Natural Hazards, Kagoshima University
1-21-40 Korimoto, Kagoshima 890-0065, Japan
E-mail: maki@rdc.kagoshima-u.ac.jp
[*2]Disaster Prevention Research Institute, Kyoto University, Kagoshima, Japan
[*3]National Research Institute for Earth Science and Disaster Prevention, Tsukuba, Japan
[*4]Graduate school, Tohoku University, Sendai, Japan
[*5]Japan Weather Agency, Tokyo, Japan
[*6]Mitsubishi Electric Co., Hyogo, Japan
[Received September 2, 2015; accepted January 19, 2016]

Preliminary results of quantitative analysis of volcanic ash clouds observed over the Sakurajima volcano in Kagoshima, Japan, were obtained by using weather radar and surface instruments. The Ka-band Doppler radar observations showed the inner structure of a volcanic ash column every two minutes after an eruption. Operational X-band polarimetric radar provides information on three-dimensional ash fall amount distribution. The terminal fall velocity of ash particles was studied by using optical disdrometers, together with the main specifications of observation instruments.

Keywords: weather radar, Sakurajima, volcanic ash cloud, ash smoke, eruption

1. Introduction

The number of explosive eruptions by the Sakurajima volcano in Kagoshima, Japan tended to increase from February 2009 and hit a record high of 996 in 2011. This rapid rise in eruptions has rapidly increased volcanic ash fall in nearby cities such as Tarumizu, Aira, Kirishima, and Kagoshima. In Kagoshima city to where, in 2012, ash fall in the observation field in Kagoshima Local Meteorological Observatory exceeded 3,500 g/m^2 [31]. This heavy ash fall has adversely affected the city by paralyzing train and car transportation. Understanding the amount of ash fall and the area affected is important in providing rapid recovery after eruptions. Because no means currently exists to get volcanic ash distribution in real time, we started in 2013 to develop weather radar based real-time ash fall estimation. In 2014 we carried out special observations in Sakurajima to measure the inner structures of ash clouds and collected the surface ground truth data [32].

While most parts of the present article are the English translation of the paper [32], additional new results and revised information are described.

Section 2 outlines special observations of Sakurajima volcano conducted in 2014 and the observation instruments used. Section 3 gives initial analysis results using observation instruments. Section 4 discusses quantitative radar-based equations for volcanic ash fall amount. Section 5 summarizes results and suggests further issues.

2. Observation

2.1. Observation Overview

To quantitatively understand whether meteorological radar detected volcanic smoke, we collected observation data on the 2013 Sakurajima eruption from X-band multiparameter (X-MP) radar, also called polarimetric radar, operated by Japan's Ministry of Land, Infrastructure, Transport and Tourism (MLITT). Here, the letter X represents a wavelength of about 3 cm.

In 2014, we conducted observations of volcanic smoke by using highly sensitive research Ka-band Doppler radar [1] having high spatial resolution to observes volcanic ash columns (**Fig. 1**). Observations were also conducted using research instruments such as a small X-band polarimetric radar and aircraft and current meteorological observation instruments of the Japan Meteorological Agency such as airport Doppler radar (not shown in **Fig. 1**). Particle size distribution data on volcanic smoke are necessary to interpret radar observation data and quantitative volcanic ash fall estimation algorithms, and ground volcanic ash fall data are necessary to verify their accuracy. We obtained data through observations using paper cups, electronic scales and parsivel [2] and two-dimensional video disdrometers (2DVD) [3–6], which measure particle size distribution.

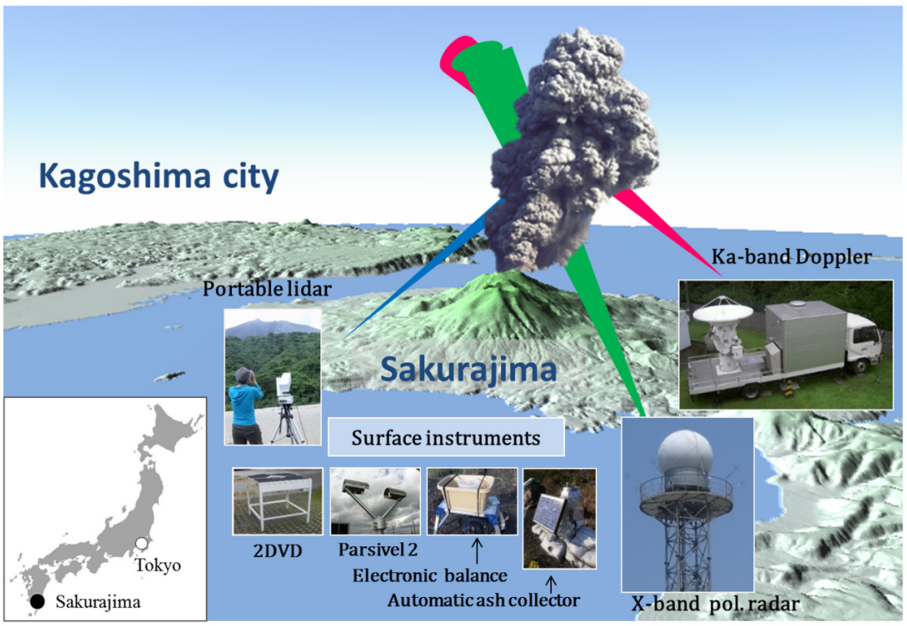

Fig. 1. Instruments used in Sakurajima volcanic ash measurements jointly-conducted with universities and research institutes.

Fig. 2. NIED Ka-band Doppler radar and portable polarization Doppler lidar at Kurokami observation station (L2 in **Fig. 7**) of Kyoto University in Sakurajima.

Table 1. Main specifications of Ka-band Doppler radar.

Code name (Site)		MP-Ka (Kurokami)
Antenna	Diameter	2.1 m (Cassegrain)
	Beam width	0.3
	Gain	54.0 dB (H)
	Scan rate (AZ)	Full Circle $\leq$ 24 deg/s
	Scan rate (EL)	-2 to $+182 \leq 12$ deg/s
Transmitter	Frequency	35.35 GHz
	Power	100 kW (Magnetron)
	PRF	400/4000 pps
	Pulse width	0.5 μs
Receiver	Smin	-107.5 dBm
	Noise figure	3.5 dB
Measured radar parameters		Z_h, V_d, σ
Max. range		30 km

The terminal fall velocity of volcanic ash particles under clam conditions was obtained through drop experiments of volcanic ash particles in a large-scale rainfall simulator of the National Research Institute for Earth Science and Disaster Prevention (NIED) [7].

The observation instruments we used in this study are detailed below.

2.2. Ka-Band Doppler Radar

Ka-band Doppler radar used in the present study was completed in 2000 by the NIED to observe the precipitation process in clouds [1]. The radar has high sensitivity to detect small particles which cm-wavelength radar cannot detect With a nationwide radio station license and carried in a 4-ton vehicle, this radar is capable of agile observation. **Fig. 2** gives an overview of the radar and **Table 1** its main specifications. We continuously observed the Sakurajima volcanic ash column from March 29 to June 8, 2014, with Ka-band Doppler radar setting at Kurokami Observation Point of the Sakurajima Volcano Research Center, Disaster Prevention Research Institute (DPRI), Kyoto University, which is 3.6 km away from Sakurajima's Showa crater. The radar, connected to the NIED via a network of Kyoto University, provides remote radar operation and data transfer. Transferred radar data were processed in nearly real time and radar observation images were opened to research community from the web site.

Antenna scan mode is based on a Plan Position Indicator (PPI) scan at an elevation angle of 16° to observe the horizontal section of the volcanic ash column and Range Height Indicator (RHI) scans at azimuth angles of 257°, 259°, 261°, and 263° for observing the vertical structure. One scan series took about 2 minutes. Spatial resolution of observed data is 75 m in a range direction. The beam

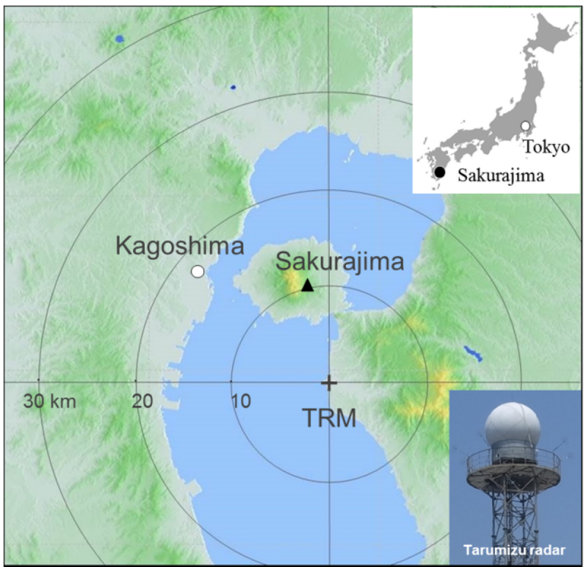

Fig. 3. Location and observation range of X-band polarimetric radar.

Fig. 4. X-band polarimetric radar at Tarumizu and Sakurajima Volcano.

Table 2. Main specifications of X-band polarimetric radar.

Code name (Site)		TRM (Tarumizu)
Antenna	Diameter	2.2 m
	Beam width	1.0°
	Gain	44.7 dB (H), 45.1 dB (V)
	Speed	1-4 rpm
	Scan angle , PPI	1.7°- 20.0° (12 tilts)
Transmitter	Frequency	9770 MHz
	Power	200 W
	PRF	1500/2000 pps
	Pulse width	1.0 μs, 32μs
Receiver	Sin	-109.5 dB
Measured radar parameters		Z_h, Z_v, Z_{DR}, Φ_{DP}, ρ_{hv}, V_d, σ
Resolution		Range : 150 m Azimuth : 1.0°

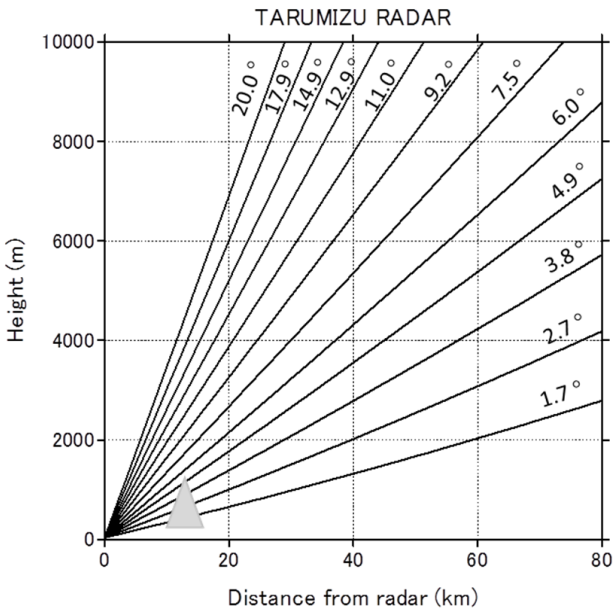

Fig. 5. Antenna scans strategy of X-band polarimetric radar. The triangle shows Sakurajima volcano.

widths are about 20 m if the antenna elevation angle is 16° over the crater and about 40 m if this angle is 60°. We acquired data on the reflectivity factor, Doppler velocity, and spectrum width.

2.3. X-Band Polarimetric Radar

X-band polarimetric radar referred as XMP radar that the MLITT launched operation in 2013 as a Sakurajima debris flow countermeasure. The MLITT set up 39 of these radars in major cities and provides rainfall information every one minute. The radar in Tarumizu city in Kagoshima obtains rainfall data within a 60 km radius (**Fig. 3**).

Figure 4 shows X-band polarimetric radar and **Table 2** lists main radar specifications. The radar's dual polarization function is used to estimate rainfall amounts and precipitation particle size distribution. The antenna scan elevation angle ranges from 1.7° to 20.0°, as shown in **Fig. 5**, observing the PPI for 12 elevation angles. Volume data are obtained within 5 minutes. Note, however, that the beam reaches maximum altitude of about 4 km above sea level over Sakurajima shown by a gray triangle in **Fig. 5**.

2.4. Portable Polarization Doppler Lidar

The portable polarization Doppler lidar was prototyped in 2011 by Mitsubishi Electric Corporation by providing a small Doppler lidar [8] with a receiving circuit unit which separates received light into depolarization and non-depolarization components. A PC was used to process signals. **Table 3** lists main specifications. **Fig. 6** is a scene of volcanic smoke observed at Arimura on Sakurajima (L6 in **Fig. 7**). Volcanic smoke was observed flexibly on Sakurajima Island between January 27 and February 14 and between May 15 and May 21, 2014.

Table 3. Main specifications of portable polarization Doppler lidar.

	Specification
Wavelength	1.54μm
Scan	AZ: -90° ∼ +90° EL: ° ∼+90°
Scan speed	AZ: ∼20° /s EL: 1∼10° /s
Output	Backscatter S/N, Depolarization degree Doppler velocity, Spectrum width
Range resolution	30m/75m/150m
Observation range	40m∼600m (30m resolution) 75m∼1500m (75m resolution) 150m∼3000m (150m resolution)
Power	AC100V 400VA
Environment	Antenna: -20∼+40° (W.proof IPX2) Body: ∼+40° (No W. proof)
Weight	Antenna: 13kg, Body: 30kg

Fig. 6. Portable polarization Doppler lidar observations at Arimura site (L6 in **Fig. 7**) in Sakurajima.

The portable polarization Doppler lidar measurement principle was as follows: Transmitted light is linearly polarized on the polarization plane and emitted from the optical transmitter and receiver into the atmosphere via the receiving circuit and optical antenna. After passing through the optical antenna, light backscattered by microparticles in the atmosphere is dispersed at the receiving circuit into the non-depolarization component in the same way as for the polarization plane of transmitted light and the orthogonal depolarization component. Spectral analyses were then conducted independently for both, and information such as the backscatter signal to noise ratio (S/N), depolarization ratio, Doppler velocity, and velocity width calculated and saved on hard disk. Depolarization ratio (δ) is the ratio of the light-receiving depolarization component, P_s, having a polarization plane perpendicular to the polarization plane of transmitted light with respect to received non-depolarization light component, P_p, having the same polarization plane as that of transmitted light. Depolarization ratio (δ) is defined by

$$\delta = qP_s/P_p \quad \ldots\ldots\ldots\ldots\ldots\ldots \quad (1)$$

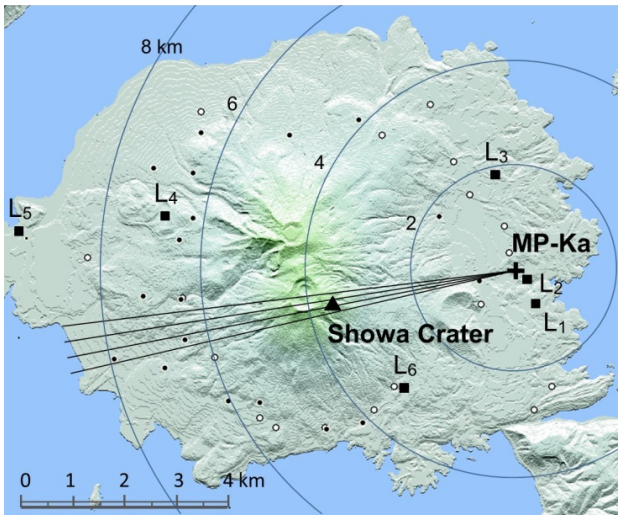

Fig. 7. Location and observation range of Ka-band Doppler radar. Black rectangles (L1-L6) are sites for agile lidar observations. White and black dots are automatic weight measurement systems for volcanic ash and drum can ash collectors, respectively. Four radial lines are azimuth angles of RHI antenna scanning.

Fig. 8. Parsivel 2 at Furusato station of Kyoto University in Sakurajima.

where, q is the sensitivity ratio of light-receiving devices of vertical and horizontal components. The depolarization ratio is the parameter that effectively determines whether a scattering particle is spherical. P_s takes a value of almost 0 for spherical particles and 0.3 to 0.7 for yellow dust, which consists of non-spherical particles.

Since this system is small, the sensor, signal processor, PC, etc., are installed in a vehicle and moved to the observation site. The vehicle battery powers all of the devices.

2.5. Laser-Optical Disdrometer

A laser-optical disdrometer is a particle size distribution measurement device that uses a laser [2]. We used an improved parsivel called Parsivel 2, developed by OTT (**Fig. 8**). **Table 4** lists main Parsivel 2 specifications.

Table 4. Main specifications of Parsivel 2.

	Specification
Wavelength	780 nm
Transmitter	0.5 mW Laser Class: 1 (21 CFR 1040.10 1040.11) 1 (IEC/EN 60825-1 A2:2001)
Sampling area	180 × 30 mm (54 cm^2)
Target	Water drop: 0.2 mm∼5 mm Solid particle: 0.2 mm∼25 mm Speed: 0.2 m/s∼20 m/s
Sampling time	10 sec∼60 min
Power	10∼28 VDC (sensor), 1.5W 12/48 VDC (heater), 50/100 W

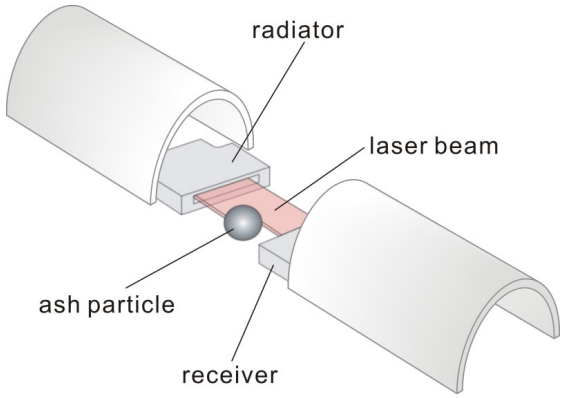

Fig. 9. Sensor area of Parsivel 2 (Catalogue figure was modified).

Parsivel 2 uses a horizontal slab-like laser beam measurement face of 180 cm × 30 cm formed between light emitter and the light receiver (**Fig. 9**). The voltage drop occurring when falling particles pass through the measurement face is measured, together with its duration time, and particle diameters and drop velocities of falling particles are calculated in real time. The number of particles included in an arbitrary-sized class where particles pass through the laser beam sheet per unit area and unit time is calculated as follows:

$$ND_{\mathrm{at}} = \frac{n}{v\delta S\delta t\delta d} \quad \cdots\cdots\cdots\cdots (2)$$

where, n is the number of particles included in the arbitrary-sized section, v is the drop velocity, δS is an area of the laser sensor, δt is time section width, and δd is size section width. Particle size distribution is obtained from NDat calculated in each size section.

Tokay et. al. [9] compares measurement to that of Parsivel 2, the first Parsivel, an impact disdrometer [10], etc. They concluded that Parsivel 2 has more advantages than the first parsivel in the following respects: First, rainfall measurement accuracy is improved. Second, Parsivel 2 is improved to measure small particle diameters more accurately. Third, drop velocity measurement error of a particle with a diameter of 1 mm or less was acceptable. The value of drop velocity at about 1 ms^{-1} was underestimated, however the larger the particle diameter, the more this trend is reduced.

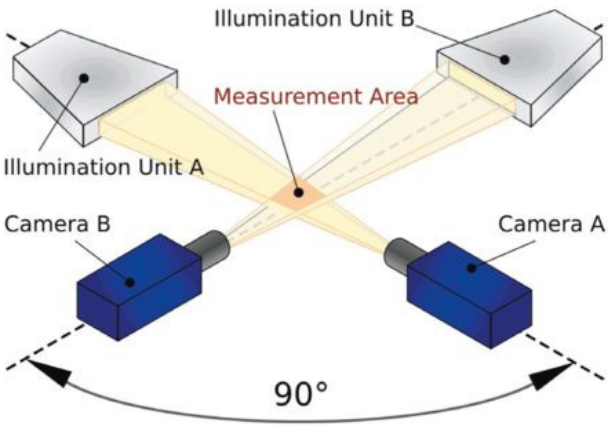

Fig. 10. Photo and Schematic of 2DVD (upper) and its measurement area (bottom) [34].

2.6. 2D Video Disdrometer

The 2DVD optical disdrometer was developed in 1991 by Joanneum Research of Austria working with the European Space Agency/European Space Research and Technology Centre (ESA/ESTEC) [3–6]. It is used to validate polarimetric radar observation because it measures raindrop shape and drop attitude in addition to raindrop size distribution and drop velocity. In 2013, the Japan Weather Association installed a 2DVD at the Sakurajima Volcano Research Center, DPRI of Kyoto University and conducted to observe volcanic ash. In 2014, they used it in volcanic ash particle drop experiments in a large-scale rainfall simulator.

Figure 10 shows the third generation 2DVD used in the present study and the measurement principle, detailed in [6]. The conventional 2DVD consisted of a sensor unit (SU), an outdoor electronics unit (OEU), and an indoor user terminal (IUT). The SU of the first 2DVD had a housing about 1.1 m high. The second-generation 2DVD has a low profile with a low housing because using the conven-

tional 2DVD could somehow affect the air flow around the housing in a strong wind, adversely affect measurement accuracy [11]. The sensor has two optical systems consisting of a line scan camera, mirror, and illuminators. The two line scan cameras are set orthogonally. The front of each of these two cameras has a 10 cm wide linear light source for detecting raindrops: raindrops dropping on the 10×10 cm measurement area formed by the two light sources block out light sources, and their shadow is detected by photodetection elements arrayed in a line inside the camera, which makes 40 kHz scans. The two light sources, i.e., the heights at which line scan cameras are mounted, differ 6.2 mm vertically, so when raindrop shadows detected by each camera are shot, the drop velocity and the horizontal velocity direction are calculated. Video data thus obtained give the corresponding diameter, raindrop contour, rainfall strength, and particle size distribution in addition to drop velocity. Analyzing raindrops contour data obtained from the two orthogonal directions gives two canting angles for each shooting angle [5, 12] and the true angle of the raindrop axis of symmetry is obtained from these two angles. This angle is expressed by declination from the vertical axis and azimuth angle.

2.7. Automatic Volcanic Ash Weight Measurement

The instrument that automatically weighs, or measures, volcanic ash was developed jointly by Nippon Koei Co., Ltd., and the Incorporated Administrative Agency Public Works Research Institute to continuously observe volcanic ash [13–16]. The instrument began operating at two sites at Sakurajima in 2008, and has continuously observed 18 sites at one-hour intervals since 2014.

The measuring instrument is shown in **Fig. 11**, and the principle behind the automatic weighing volcanic ash is shown in **Fig. 12**. The system's measurement section consists of a cylindrical ash tank 30 cm high and having an internal diameter of 20 cm. The tank contains a floating magnetostrictive water level sensor and is supported by a load cell [13].

The measurement mass obtained by the load cell and measurement water head level obtained by the water gauge are used to calculate ash deposition mass (W_s) and deposition thickness (L) with the following equations [16]:

$$W_s = (W - S \cdot D \cdot \rho_w)/(1 - \rho_w/\rho_s) \quad \ldots\ldots \quad (3)$$

$$L = W_s/(S \cdot \rho_d) \quad \ldots\ldots\ldots\ldots \quad (4)$$

W: tank content weight, S: tank opening, D: water level, ρ_w: water density, ρ_s: volcanic ash soil particle density, ρ_d: apparent volcanic ash layer deposition density. We used 2.64 gcm^{-3} for ρ_s based on the soil particles of volcanic ash deposited around the observation site. We used 1.50 gcm^{-3} for ρ_d based on the measurement of deposited volcanic ash layers.

Automatic weighing of volcanic ash involves two automatic drain valves: one for filter transmission and the other to prevent water overflow.

The first drain valve is activated at setup and drains a set water head level. Water drained through the tank bottom after penetrating the volcanic ash layer in the tank is used to calculate the hydraulic conductivity of the volcanic ash layer.

The second drain valve prevents water from overflowing by draining water from the bottom of the water gauge if water exceeds a certain level. The rainfall amount is measured automatically based on changes in the water level by these two types of drainage.

A solar panel and battery supply electricity. Data communication is conducted by a mobile phone at fixed times. On the lower measurement section is a 30 by 30 cm stainless steel storage box that contains a data recorder such as a data logger, a battery, a mobile phone, a power supply, a communication section, etc.

Fig. 11. Automatic weight measurement system for volcanic ash.

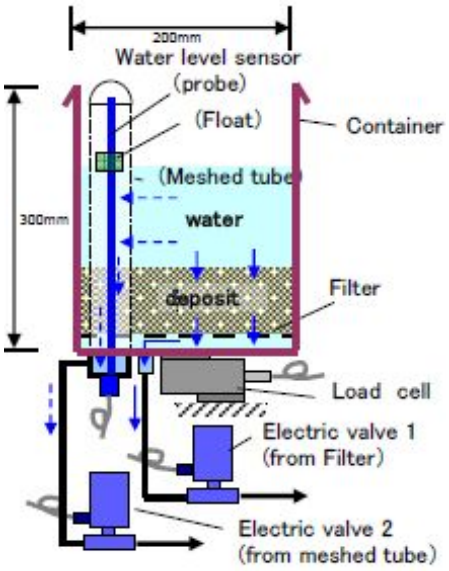

Fig. 12. Principle of automatic weight measurement system for volcanic ash [16].

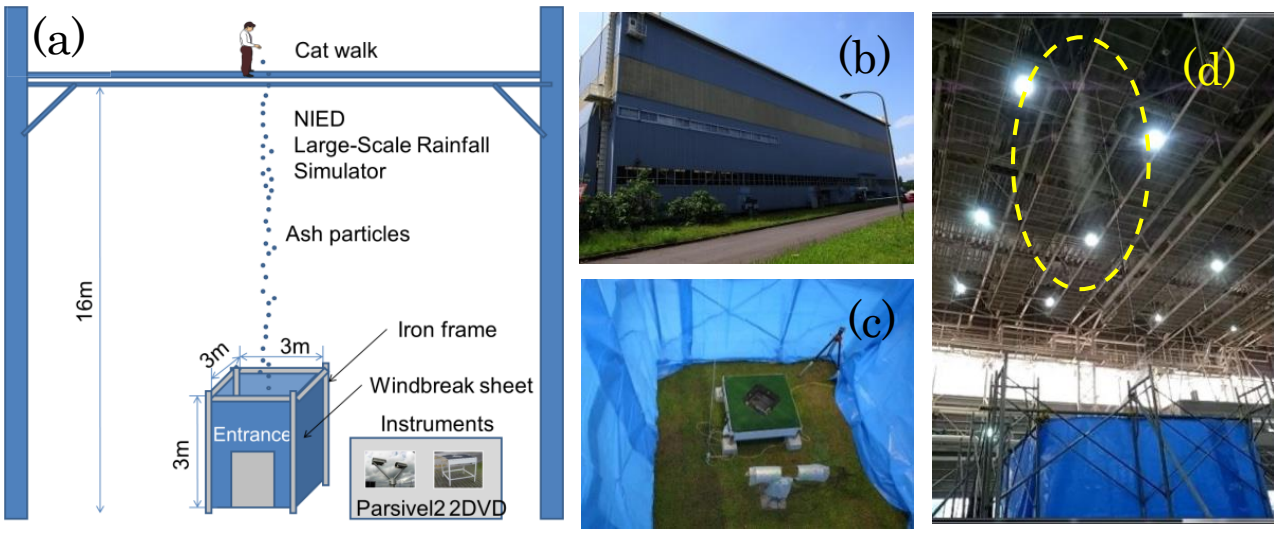

Fig. 13. (a) Schematic image of the experiment, (b) NIED rain simulator, (c) experimental area for 2DVD and Parsivel 2, and (d) falling volcanic ash particles.

2.8. Freefall Ash Particle Experiments

We collected volcanic ash samples at multiple sites and measured ash terminal fall velocities and particle size distribution necessary for estimating ash fall quantitatively. For measurement, we used a large-scale rainfall simulator (**Fig. 13**) of the NIED to ensure fall height sufficient for a water drop to reach terminal velocity. Experiments involved simultaneous measurement conducted using the 2DVD and an electronic balance in addition to Parsivel 2.

Experiments were conducted using two types of volcanic ash from Sakurajima. One consisted of 13 samples sifted in advance and sorted into six particle sizes, i.e., 0.125 to 0.25, 0.25 to 0.50, 0.50 to 1.0, 1.0 to 2.0, 2.0 to 4.0, and 4.0 to 8.0 mm. The other consisted of 54 samples collected in February, March, and April of 2014 at the 18 sites where automatic ash weight measurement systems of the MLITT were installed. In conducting drop experiments for these 67 volcanic ash samples, we dropped sample particles stimulating their dispersion by taking about 30 seconds to drop about half of a cup of samples. Measurement lasted 1 minute. After confirming that particles had been measured by instruments sufficiently then measured the next particle sample. For samples with known particle diameters, we conducted 3 or 4 drop experiments per sample and calculated the drop fall velocity.

3. Results

3.1. Ka-band Doppler Radar Observation

We observed volcanic ash columns from March 29 to June 8, 2014 using the NIED Ka-band radar set up at the Kurokami observation site of the DPRI, 3.6 km from Sakurajima's Showa crater. Observations were based on sector PPI scans of the horizontal structure of a volcanic ash column at an elevation angle of 16° and sector RHI scans of the vertical structure at azimuth angles of 257°, 259°, 261°, and 263°. These series of observations took about 2 minutes. The spatial resolution of observations was 75 m in the range direction. The beam was about 20 m wide at an elevation angle of 16°. We obtained data on the reflectivity factor, Doppler velocity, and spectrum width of a volcanic ash column.

A total of 77 eruptions, including 49 explosive eruptions, occurred during observation according to the Japan Meteorological Agency [33]. Among these, we obtained data on 53 eruptions, 35 of which were explosive. These also include two cases in which the volcanic ash column reached a height of 4,500 m above the crater and one that reached 3000 m. These also included 14 cases in which volcanic smoke altitude was unknown because the volcanic ash column was contaminated with rainfall or clouds.

A typical example of radar analysis results for the volcanic ash column is shown in a Ka-band radar image of the explosive eruption at 13:07 on May 10, 2014 (**Fig. 14**). The ash column was about 1 km wide directly above the crater 2 minutes after the eruption, diffusing 2 km east and west and 3 km north and south after 10 minutes (**Fig. 14**). RHI observation successfully captured ash volume time changes. The upward velocity of the ash column echo top was 37 ms^{-1} after 20 seconds, 30 ms^{-1} after 40 seconds, and 25 ms^{-1} after 60 seconds after the eruption. Within 2 minutes, they had decelerated to about 18 ms^{-1} and in 5 minutes to about 7 ms^{-1}. The highest altitude of the ash column reached 5200 m above sea level. According to visual observation by Japan Meteorological Agency personnel, the ash column was 5300 m above sea level, therefore differing from that of RHI observation by about 100 m. The ash column altitude observed by radar is the sum of the center altitude of the radar beam with a distance of half width of the beam.

Figure 15(a) presents the vertical distribution north of the ash column center of the column's reflectivity factor 4 minutes after eruption. Content is not uniform and

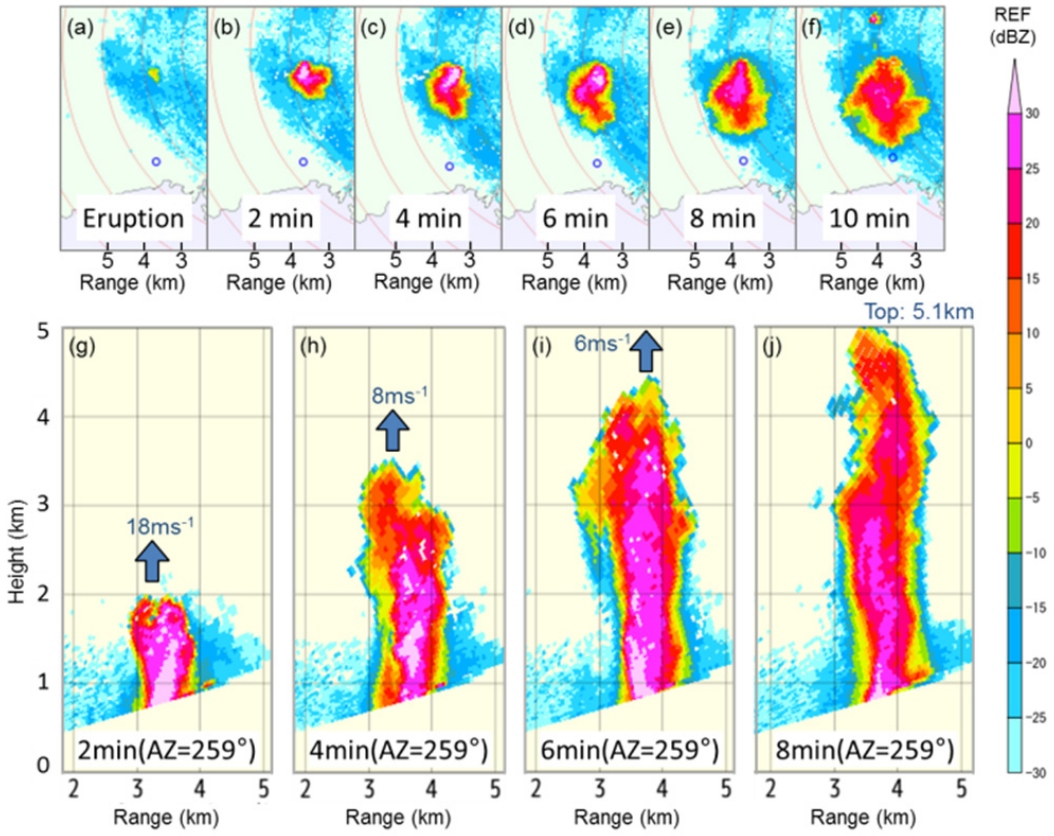

Fig. 14. Time change of Ka-band radar reflectivity of volcanic ash column after explosive eruption. PPI image at the elevation angle of 12° (above), RHI image (below). 13:07JST, May 10, 2014.

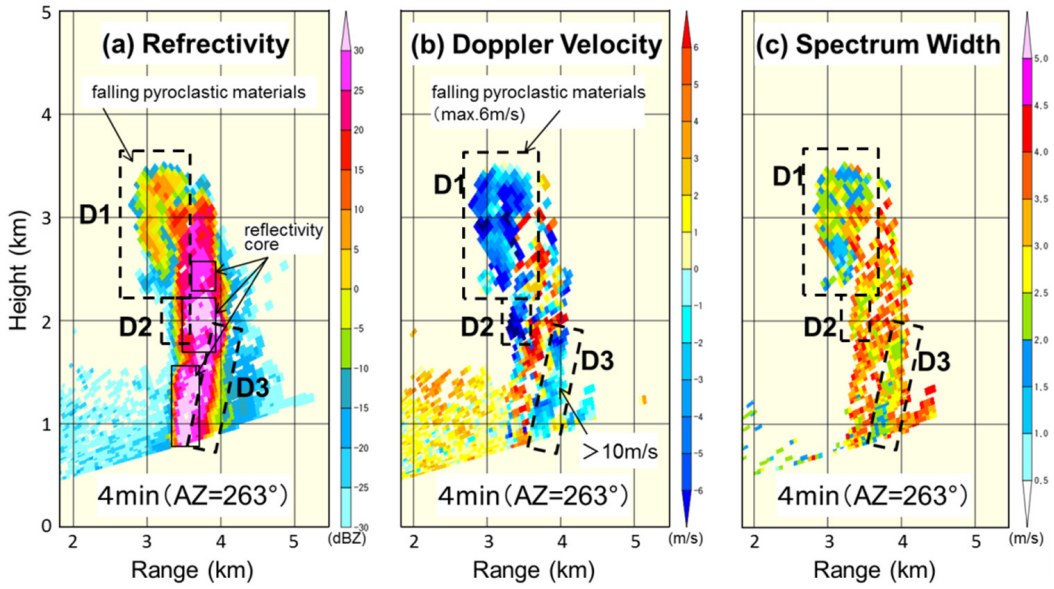

Fig. 15. RHI image of (a) Reflectivity (dBZ), (b) Doppler velocity (ms^{-1}), and (c) Doppler spectrum width (ms^{-1}) 4 minute after volcanic eruption. 13:11JST, May 10, 2014.

includes ZH cores at 3 points corresponding to positive Doppler velocity (upflow) (**Fig. 15(b)**). Upward velocity estimated ignoring the effect of horizontal wind was about 4 ms^{-1}. Negative Doppler velocity (downflow) was observed in areas enclosed by dashed lines D1, D2, and D3. In D1, particularly, downward velocity was observed up to 6 ms^{-1}. The reflectivity factor distribution of D1 is so characteristic that it is considered to reflect the dropping of clastics. Downflow was dominant for most altitudes 10 minutes after the ash column reached its maximum

altitude (not shown). Distribution of the Doppler spectrum width (**Fig. 15(c)**), which is an index of turbulence strength, indicates that positive Doppler velocity (upflow) is high and negative Doppler velocity (downflow) is low.

3.2. X-Band Polarimetric Radar Observation

We analyzed observation data from MLITT X-MP radar for the same eruption cases as discussed in the previous section. Although resolution as high as Ka-band Doppler radar is not possible, 3D polarization parameter distribution data at intervals of 5 minutes can be analyzed. Horizontal (**Fig. 16(a)**) and vertical (**Figs. 16(b)(c)**) distribution of vertically integrated reflectivity (VIR) was obtained for the 43 minutes from 13:12 to 13:55JST, 2014 using a 3D analysis tool [17] now being developed by Kagoshima University.

As **Fig. 16(a)** indicates, the VIR time integration value is maximum at about 500 m south from the Showa crater and the distribution width becomes wide enough to reach slightly westward over the sea about 6 km from the crater. The vertical cross-section along line A-B indicates that VIR is maximum at an altitude of about 1500 m from the altitude where radar is installed, i.e., about 700 m from the Showa crater. The vertical-cross section along line C-D indicates that the distribution width reaches a maximum of 3.5 km at an altitude of about 2500 m, i.e., about 1700 m from the crater.

Note that **Figs. 16(a)** and **(b)** exhibit northward distribution patterns from Showa crater. These are thought to be due to a spurious echo caused by the range side lobe of transmitted pulse.

3.3. Portable Polarization Doppler Lidar Observation

We conducted 27 observations between January 27 and February 14, 2014. Those from January 27 to 30 were 11 agile observations, i.e., L1, L3, L4, and L5 in **Fig. 7**. The time for one observation varied case by case, e.g., a short observation took about 1 minute and a long one about 3 hours. From January 31 to February 14, we conducted automatic 24-hour observation in the direction of the crater at a fixed point (L2 in **Fig. 7**). Between May 15 and 21, we obtained data by agile observation (L2 and L6 in **Fig. 7**) with the objective of observation synchronized with Ka-band Doppler radar.

The data thus acquired are now being analyzed. An example of ash smoke observed at 11:08 Japan Standard Time on January 28 is presented in **Fig. 17**. Although no eruption was reported in this case, we successfully recorded volcanic smoke emitted continuously from the crater. Nondepolarization component distribution (**Fig. 17(a)**) indicates that volcanic smoke echo emitted from the crater meanders northwards. Depolarization component strength distribution (**Fig. 17(b)**) indicates that this is an echo of the volcanic smoke. The Doppler velocity distribution pattern is shown in **Fig. 17(c)**. Although the detailed distribution of wind direction and velocity cannot be estimated from one Doppler lidar observation, the overall wind direction pattern is consistent

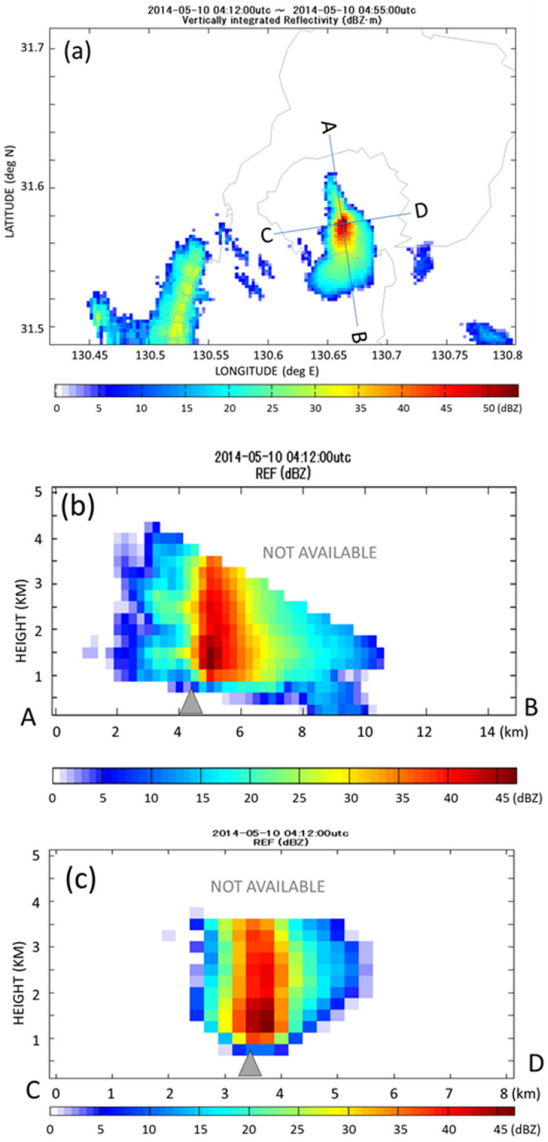

Fig. 16. (a) Horizontal distributions of vertically integrated reflectivity, (b) vertical cross section along the line A-B, and (c) vertical cross section along the line C-D.

with wind information from the Kagoshima Local Meteorological Observatory (**Fig. 17(d)**). The polarization Doppler lidar detects small particles not acquirable by microwave radar, so it can estimate volcanic smoke height effectively and detect micro particles that may cause serious problem to aircraft operation.

3.4. Quantitative Radar Ash Fall Estimation

Based on volcanic ashfall rate R_A ($\mathrm{kgm^{-2}h^{-1}}$) measured on the ground surface and radar reflectivity factor Z ($\mathrm{mm^6m^{-3}}$) measured above the same ground, ashfall rate estimation equation ($R_A - Z$ relationship) is obtained. It is extremely rare for a momentary R_A value to be measured, so what is usually obtained is information on integrated volcanic ash fall investigated on the ground after an eruption. We obtained the $R_A - Z$ relationship as follows from ground integrated volcanic ash fall and integrated radar reflective factor information.

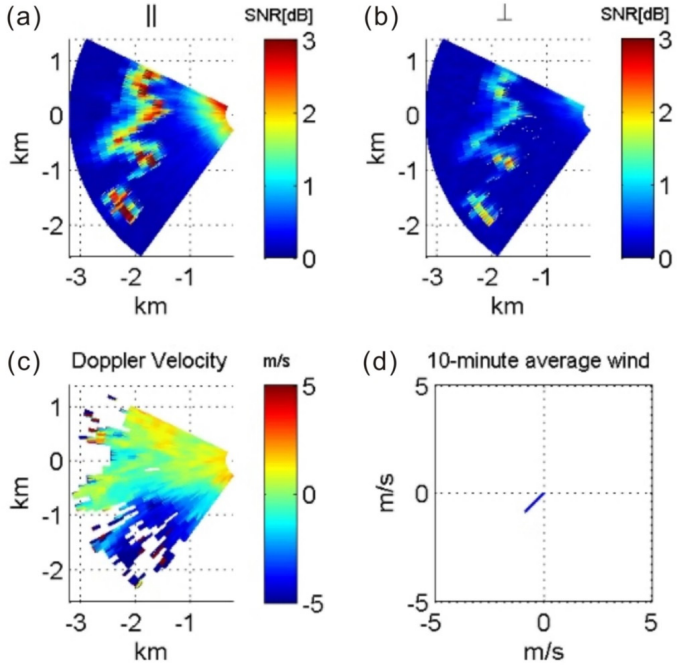

Fig. 17. An example of ash smoke observed by a potable polarization Doppler lidar at L3 in **Fig. 7**: (a) non- depolarization component, (b) depolarization component, (c) Doppler velocity, and (d) wind direction from JMA.

Let the $R_A - Z$ relation be expressed by the following exponentiation formula:

$$R_A = \alpha Z^{\beta} \quad \ldots\ldots\ldots\ldots\ldots\ldots (5)$$

We assume that the $R_A - Z$ relation does not change in time or place, i.e., α and β do not change temporally. Taking the logarithm of Eq. (5), we integrate it on $T(h)$, which is the period in which volcanic smoke was observed,

$$\int_0^T 10\log R_A dt = T \cdot 10\log\alpha + \beta \int_0^T 10\log Z dt \quad (6)$$

If R_A is constant with time in the left-hand member of Eq. (6), S_A (kgm^{-2}), which is the time integration value of R_A, is

$$S_A = \int_0^T R_A dt = T \cdot R_A \quad \ldots\ldots\ldots\ldots (7)$$

Take the logarithm of the above expression and deform it into

$$\int_0^T 10\log R_A dt = T \cdot 10\log(S_A/T) \quad \ldots\ldots (8)$$

Time integration value S_Z (dBZh) of reflectivity factor $10\log Z$ (dBZ) is

$$S_Z = \int_0^T 10\log Z dt \quad \ldots\ldots\ldots\ldots (9)$$

Assign Eqs. (8) and (9) to Eq. (6) to get

$$10\log(S_A/T) = 10\log\alpha + \beta(S_Z/T) \quad \ldots\ldots (10)$$

Let integrated volcanic ash falls measured at observation points 1, 2, …, and n be S_{A1}, S_{A2}, …, and S_{An}, then let observed integrated reflectivity factors be S_{Z1}, S_{Z2}, …, and S_{Zn}, and integrated times be T_1, T_2, …, and T_n. Coefficients α and β of Eq. (10) are obtained by the least squares method from the scatter diagram of ($S_A i/T_i$, $S_Z i/Ti$); $i = 1, n$. This enables an equation for estimating volcanic ashfall rate to be obtained from radar observation using an observation value of ground volcanic ash fall as ground truth data. This type of procedure is called the engineering approach [18].

At present, we have collected data from X-MP radar and automatic ash weight measurement from the MLITT at Sakurajima for 31 eruptions in 2013 having a volcanic smoke altitude of 3000 m or higher and are developing a volcanic ash fall estimation equation for each case.

For the August 18, 2013, eruption, we obtained the following provisional expressions:

$$10\log(S_A/T) = 2.72 + 0.0207 \times (S_Z/T) \quad . \quad (11.a)$$

$$R_A = 1.87Z^{0.0207} \quad \ldots\ldots\ldots\ldots (11.b)$$

These relationships assume that R_A on the left side of Eq. (6) is constant over time, although the validity of this assumption is still being verified.

In an example of past analysis conducted the same way, we derived the following expression regarding the Shinmoedake eruption from January 26 to January 27, 2011 [19].

$$R_A = 1.29Z_H^{0.0499} \quad \ldots\ldots\ldots\ldots (12)$$

3.5. Distributions of Accumulated Radar Reflectivity

The amount of volcanic product is estimated from ground deformation observation data [20]. Specifically, the discharge volume of volcanic ash is estimated from contraction volume of the pressure source observed immediately after an explosive eruption. According to statistical analyses, the prediction accuracy of final strain which is an important parameter for estimating contraction volume, is about 10% for individual explosive eruptions by Sakurajima [21]. This means that the ash discharge volume can be estimated with a certain accuracy. In the case of explosive Showa crater eruptions, for which the ash discharge volume of individual eruptions is estimated using data from the ground volcanic ash fall observation point on Sakurajima Island, the volume of volcanic ash discharged in a large explosive eruption is estimated to be several tens of thousands of tons, but are mostly 10,000 tons [22].

In this study, we are trying to estimate volcanic ash fall for individual eruptions by comparing crustal movement, e.g., initial or final strain, with an X-MP radar reflectivity factor for individual eruption cases. For this purpose, we calculated the time integration value of PPI data of reflectivity factor at 6 degree elevation angle for each case in 2013 where the volcanic smoke altitude was 3000 m or higher. **Fig. 18** shows an example of the distribution of the integrated reflectivity factor of the largest eruption, on August 18, 2013. The integrated reflectivity factor distributes northwest from the Showa crater into Kagoshima city. The maximum value appears at about 500 m just southwest of the Showa crater. The second biggest value appears about 2 km west of the Showa crater.

3.6. Terminal Velocity Measurements in an Artificial Rainfall Simulator

We dropped volcanic ash samples from a height of about 17 m at the NIED's large-scale rainfall simulator and measured particle size distribution and ash particle drop velocity. using a Parsivel.

The relationship between particle diameter and drop velocity obtained from a Parsivel 2 measurement is presented in **Fig. 19**. The relationship between the particle diameter and the drop velocity obtained by the least squares method assuming an exponentiation function is

$$v = 5.90D^{0.530} \quad \ldots\ldots\ldots\ldots \quad (13.a)$$

The relational expression assuming a logarithmic function is

$$v = 4.468 \ln D + 6.036 \quad \ldots\ldots\ldots \quad (13.b)$$

The relational expression of the exponentiation function obtained from 2DVD measurement results in the same experiment is

$$v = 6.25D^{0.50} \quad \ldots\ldots\ldots\ldots \quad (13.c)$$

This relational expression agrees well with relational expression Eq. (13.a) obtained from Parsivel 2. The expression using a logarithmic function is

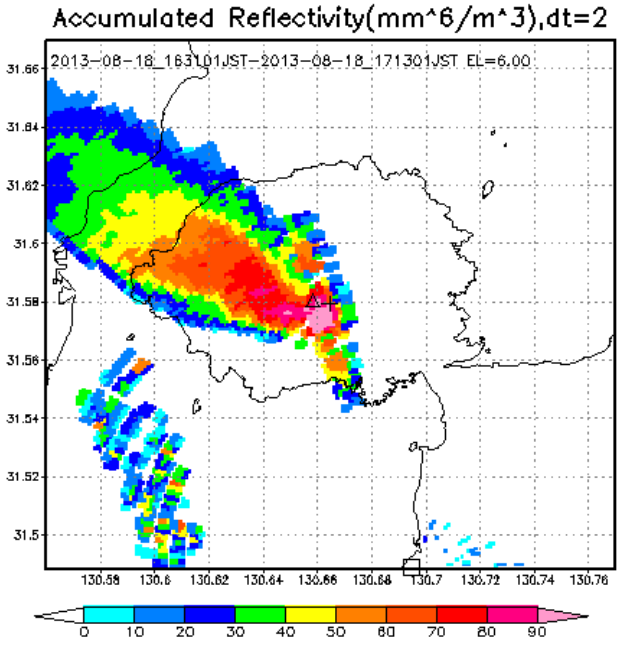

Fig. 18. Distribution of accumulated reflectivity (16:31-17:13JST, August 18, 2013). △: Minamidake, +: Showa crater.

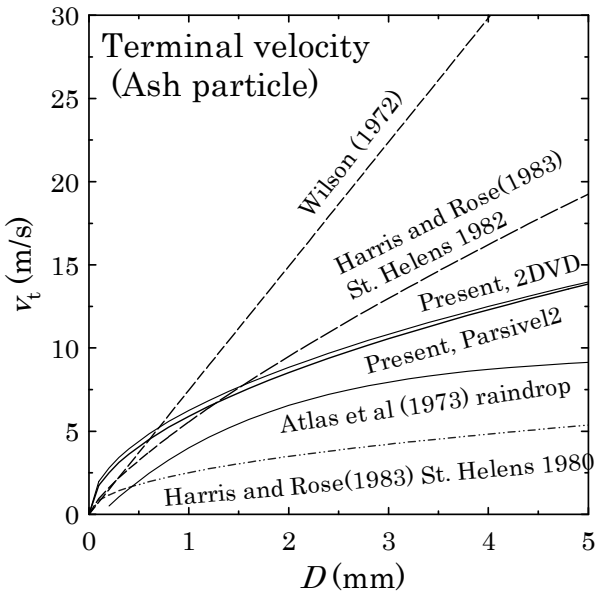

Fig. 19. Relationship between the terminal velocity and diameter obtained from Parsivel 2 and 2DVD.

$$v = 4.143 \ln D + 5.275 \quad \ldots\ldots\ldots \quad (13.d)$$

The above expressions do not necessarily give terminal velocities for all particle diameters because drop experiments were conducted from a height of about 17 m, and large "solid" particles are less likely to have reached terminal velocity by the time they reached the ground.

Based on an examination of past literature for terminal velocities estimated in actual past eruptions, we obtained the following relational expressions by putting the exponentiation expression into ash drop velocity data [23] of volcanic in the 1980 and 1982 eruptions of Mount St He-

lens in the US state of Washington.

$$v = 2.51D^{0.472} \quad \text{St Helens 1980} \quad \ldots\ldots \quad (14.a)$$

$$v = 5.56D^{0.772} \quad \text{St Helens 1982} \quad \ldots\ldots \quad (14.b)$$

Above equations are similar to those obtained in previous paper [24]. With reference to results [25] for a theoretical model of particles falling pyroclastically [23, 24], we obtained the following equation.

$$v = 7.46D \quad \ldots\ldots\ldots\ldots \quad (14.c)$$

Comparing experiment expression Eq. (13.a) obtained by this study to St. Helens measurements, the experimental expression is consistent as long as the particle diameter is up to about 2 mm. As a reference, **Fig. 19** presents an empirical equation [26] of rain particle drop velocity. Overall, volcanic ash particle drop velocity is greater than that of raindrops.

Using the drop velocity equation obtained by Parsivel 2 in this study, we verified the particle size distribution of samples with a known particle diameter [7]. The obtained particle size distribution reflected the known particle diameter well. The peak particle size distribution was identified to be almost the same particle diameter as that in samples with a particle diameter of 0.125 to 0.25 mm and 0.25 to 0.5 mm. This is because the minimum Parsivel 2 particle diameter is 0.2 mm.

We concluded that for a sample in which most particles have a diameter of 0.2 mm or more, Parsivel 2 analysis of particle size distribution is effective for volcanic ash falls.

The above results are based on laboratory analysis, but we observed volcanic ash particles in actual eruptions conducted at the DPRI Furusato Observation Site on Sakurajima. Some data for eruption cases have been obtained and initial analysis results have been introduced [27].

4. Discussion

Section 3.4 includes the derivation of an ash fall estimation equation using the so-called engineering approach. In a scientific approach based on particle size distribution information on volcanic ash particles, we derived a volcanic ash fall estimation equation for Sakurajima using a previous study [28] as a reference and applied it to actual observation data.

We assumed that the ash particle size distribution took the following function form [28, 29]:

$$N_A(D) = N_n \left(\frac{D}{D_n}\right)^{\mu} e^{-\Lambda_n \left(\frac{D}{D_n}\right)^{\nu}} \quad \ldots\ldots \quad (15)$$

D (mm) is particle diameter; D_n (mm) average diameter weighted by the number of particles; N_n (intercept factor), Λ_n (slope factor) and μ (shape factor) – parameters characterizing particle size distribution. The above equation is simplified into two, i.e., normalized Weibull distribution ($\nu = \mu + 1 = 3\gamma + 3$) and normalized Gamma distribution ($\nu = 1$). Based on an analysis of actually measured volcanic ash particles, $\mu = 1$ for the normalized Weibull distribution and $\mu = 0.5$ for the normalized Gamma distribution. Let ash particles (solid) density be ρ_A (gm^{-3}), sphere-equivalent mass be m_A (g), and ash mass density C_A (kgm^{-3}) expressed by the following equation:

$$C_A \equiv 10^{-3} \int_{D_1}^{D_2} m_A(D) N_A(D) dD = \frac{10^{-3}\pi}{6} \rho_A m_3 \quad \ldots\ldots\ldots\ldots\ldots\ldots \quad (16)$$

D_1 and D_2 are minimum and maximum diameters (mm). m_3 is the third-order moment of particle size distribution. Average diameter D_n weighted by the number of particles is expressed as follows:

$$D_n = \frac{\int_{D_1}^{D_2} D N_A(D) dD}{\int_{D_1}^{D_2} N_A(D) dD} = \frac{m_1}{m_0} \quad \ldots\ldots\ldots \quad (17)$$

If $D_1 = 0$ and $D_2 = \infty$, the particle distribution of the normalized Weibull distribution ($\mu = 3\gamma + 2$) is

$$\begin{aligned} m_n &= \int_{D_1}^{D_2} D^n N_A(D) dD \\ &= \frac{\left[\Gamma\left(1 + \frac{1}{3(\gamma+1)}\right)\right]^3 \Gamma\left(1 + \frac{n}{3(\gamma+1)}\right)}{\frac{\pi}{6} \cdot \Gamma\left(\frac{\gamma+2}{\gamma+1}\right) \cdot \left[\Gamma\left(1 + \frac{1}{3(\gamma+1)}\right)\right]^n} \frac{D_n^{n-3}}{\rho_A} C_a \end{aligned} \quad \ldots\ldots\ldots\ldots\ldots\ldots \quad (18)$$

Γ is a complete gamma function and $\gamma = -0.5$ (i.e., the normalized Weibull distribution with $\mu = 0.5$).

Volcanic ash strength R_A (kgh^{-1}m^{-2}) is expressed by the following equation expressing R_A in units of (mmh^{-1}), for which R_A/ρ_A should be used:

$$\begin{aligned} R_A &\equiv 3.6 \times 10^{-3} \int_{D_2}^{D_1} [v_A(D) - w_{up}] m_A(D) N_A(D) dD \\ &= 3.6 \times 10^{-3} \left[\frac{\pi}{6} a_v \rho_A m_{3+b_v} - w_{up} C_A\right] \end{aligned} \quad \ldots\ldots\ldots\ldots\ldots\ldots \quad (19)$$

a_v and b_v are the coefficient and the power index of the empirical equation of drop velocity of particles considering the altitude change in air density. As discussed earlier, $a_v = 5.90$ ms^{-1} and $b_v = 0.530$ based on free fall experiments for volcanic ash particles conducted at the NIED's large-scale rainfall simulator [7].

The ash particle attenuation of radio waves in case of the X-band is about 0.1 dB km^{-1}, which is negligible. When Rayleigh approximation is true, radar reflectivity factor Z_H is defined by the following equation:

$$Z_H = \frac{\lambda^4}{\pi^5 |K_a|^2} \eta_H = \int_{D_1}^{D_2} D^6 N_a(D) dD = m_6 \quad \ldots\ldots \quad (20)$$

η_H is radar reflectivity, K_a a complex dielectric factor, and λ wavelength. According to Oguchi et al. [30], the imaginary part has a slight frequency dependence and relative Sakurajima ash permittivity is $\varepsilon = 5.2729 - i0.13239$ within a range where frequency is between 3 GHz and

Table 5. Estimators of ash amount density C_A (gm^{-3}) and ash fall rate R_A ($\mathrm{kgm}^{-2}\mathrm{h}^{-1}$). Z_H ($\mathrm{mm}^6\mathrm{m}^{-3}$) is reflectivity of ash particle.

Ash particle type	fine ash ($D_n = 0.01$ mm)	coarse ash ($D_n = 0.1$ mm)	Lapilli ($D_n = 1$ mm)
Ash amount density	$C_A = 80.6 Z_H$	$C_A = 8.06 \times 10^{-2} Z_H$	$C_A = 8.06 \times 10^{-5} Z_H$
Ash fall rate	$R_A = 2.62 \times 10^2 Z_H$	$R_A = 8.86 \times 10^{-1} Z_H$	$R_A = 3.01 \times 10^{-3} Z_H$

13 GHz, i.e., an average of three measurements. The complex dielectric factor is

$$|K_a|^2 = |(\varepsilon_r - 1)/(\varepsilon_r + 2)|^2 = 0.2025 \quad . \quad . \quad . \quad . \quad (21)$$

A previous study [28] uses $|K_a|^2 = 0.39$, where frequency is between 4 GHz and 19 GHz.

Assuming normalized Weibull distribution ($\mu = 0.5$) and $w_{up} = 0$ in Eq. (19) and substituting Eq. (18) into Eqs. (16) and (19), we obtained the following equation:

$$C_A = \left(10^{-3} \frac{\pi \rho_a}{6} \frac{m_3}{m_6}\right) Z_H \cong 3.21 \times 10^{-5} \frac{\rho_A}{D_n^3} Z_H \quad . \quad (22)$$

$$R_A = \left(3.6 \times 10^{-3} \frac{a_v \pi \rho_A}{6} \frac{m_{3+b_v}}{m_6}\right) Z_H \cong 2.03 \times 10^{-4} \frac{a_v \rho_A}{D_n^{3+b_v}} Z_H \quad . \quad . \quad . \quad . \quad . \quad . \quad . \quad . \quad . \quad (23)$$

Marzano et al [28] classifies volcanic ash into fine, coarse, and lapilli, and gives $D_n = 0.01$ mm (fine ash), $D_n = 0.1$ mm (coarse), and $D_n = 1$ mm (lapilli). Following this classification, we obtained the estimation equation in **Table 5** (see also **Fig. 20**). We used experiment results [7] in a large-scale rainfall simulator for the drop velocity of volcanic ash particles and the value at Sakurajima ($\rho_A = 2.512$ gcm^{-3}) [30] for density, however. Note that Z_H in the above equation is reflectivity factor Z_{HA} of volcanic ash. For weather radar, equivalent radar reflectivity factor Z_{He} is ordinarily measured assuming raindrops. Let the dielectric factor of water be 0.93 and the dielectric factor of volcanic ash be 0.20251 [30], and Z_{Ha} is calculated by

$$Z_{HA} = (0.2025/0.93) Z_{He} = 0.218 Z_{He} \quad . \quad . \quad . \quad (24)$$

We attempted to estimate volcanic ash fall by applying the above equation to the eruption case of May 10, 2014, and we got an estimate result that greatly fluctuated depending on the value of D_n. How to estimate likely D_n remains a challenge for the future.

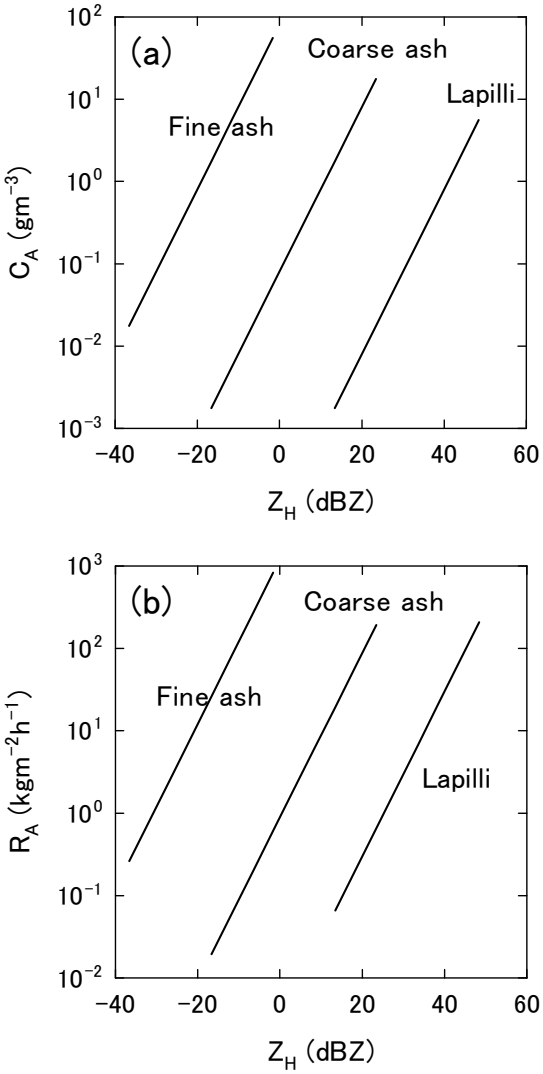

Fig. 20. (a) $C_A - Z_H$ and (b) $R_A - Z_H$ for volcanic ash clouds.

5. Summary

To establish a quantitative estimate and a prediction method of volcanic smoke amounts by weather radar, we conducted observations using ground instruments such as Ka-band research Doppler radar, currently operating X-MP radar, and Parsivel 2. Ka-band Doppler radar observation acquired a change in the internal structure of volcanic ash columns immediately after eruptions. Information on the Doppler velocity directly above the crater suggests that the eruption velocity of pyroclastic materials can be estimated. We confirmed that currently operating X-band weather radar gave useful information for quantitatively estimating volcanic ash fall. Doppler lidar observation gives distribution information on particles of several tens of microns that cannot be detected by Ka-band or X-band. These multiwavelength remote sensing observations are effective in assembling a picture of volcanic smoke. Drop experiments for volcanic ash particles that we conducted on a large-scale rainfall simulator and ground observation by Parsivel 2 at Sakurajima gave useful findings on drop velocity and ash particle size distribution necessary for estimating quantitative volcanic ash fall using radar.

Acknowledgements

In installing radar and other measuring instruments at Sakurajima and in observation, we received invaluable cooperation from Dr. Daisuke Miki of Sakurajima Volcano Research Center, DPRI of Kyoto University and Dr. Daisuke Fukushima of the Sakurajima Museum. We received data on X-MP radar and automatic volcanic ash fall data from the Kyushu Regional Development Bureau, MLITT. This study was subsidized by a general joint research grant from the DPRI of Kyoto University (25G-11), operating expense grants of the NIED, and JSPS Grant-in-Aid for Scientific Research No. 24244069 for which we hereby express our deep appreciation.

References:

[1] K. Iwanami, M. Maki, R. Misumi, S. Watanabe, and K. Hata, "The NIED dual-frequency cloud radar system under development," In Proc. 1st Int. Workshop on Spaceborne Cloud Profiling Radar, Tsukuba, Japan, pp. 161-164, 2000.

[2] M. Löffler-Mang, and J. Joss, "An optical disdrometer for measuring size and velocity of hydrometeors," J. Atmos. Oceanic Technol., Vol.17, pp. 130–139, 2000.

[3] H. E. Urban, M. Schönhuber, W. L. Randeu, and W. Riedler, "Technical Note under ESTEC/Contract No.9949/92/NL/PB(SC) – Work Order No.02 ("Development and Delivery of a 2D-Video-Distrometer")," Institute of Applied Systems Technology, JOANNEUM RESEARCH, Graz / Austria, 1994.

[4] M. Schönhuber, H. E. Urban, E. M. Richter, W. L. Randeu, and W. Riedler, "Design Review Report under ESTEC/Contract No.9949/92/NL/PB(SC) – Work Order No.02 ("Development and Delivery of a 2D-Video-Distrometer")," Institute of Applied Systems Technology, JOANNEUM RESEARCH, Graz / Austria, 1993.

[5] M. Schönhuber, G. Lammer, and W. L. Randeu, "The 2D-video-distrometer, Precipitation, Advances in Measurement, Estimation and Prediction," S. Michaelides, Ed., Springer, pp. 3-31, 2008.

[6] A. Kruger, and W. F. Krajewski, "Two-Dimensional Video Disdrometer: A Description," J. Atmos. Oceanic Technol., Vol.19, pp. 602–617, 2002.

[7] T. Miwa, M. Maki, T. Kozono, E. Fujita, T. Tanada, and M. Iguchi, "Experimental Measurement on Falling Velocity of Volcanic Ash from Sakurajima Volcano by Using PARSIVEL Disdrometer," Annuals Disas. Prev. Res. Inst., Kyoto Univ., No.58 B, pp. 91-94, 2015 (in Japanese with English abstract).

[8] S. Kameyama, T. Ando, T. Yanagihara, H. Sakamaki, T. Wakayama, Y. Hirano, M. Furuta, M. Hagio, and Y. Fujii, "Winds measurements with earth environment survey laser – Application of cohelent Doppler lidar in various area," Inspection Engineering, Vol.9, No.8, pp. 25-29, 2004 (in Japanese).

[9] A. Tokay, D. B. Wolff, and W. A. Petersen, "Evaluation of the New Version of the Laser-Optical Disdrometer OTT Parsivel," J. Atmos. Oceanic. Technol., Vol.31, pp. 1276-1288, 2014.

[10] J. Joss, and A. Waldvogel, "Ein Spektrograph fur Niederschlagstrophen mit automatischer Auswertung," Pure Appl. Geophys., Vol.68, pp. 240-246, 1967.

[11] V. Nespor, W. F. Krajewski, and A. Kruger, "Wind-induced error of raindrop distribution measurement using a two-dimensional video disdrometer," J. Atmos. Oceanic Technol., Vol.17, pp. 1483–1492, 2000.

[12] G-J. Huang, V. N. Bringi, M. Thurai, "Orientation Angle Distributions of Drops after 80 m fall using a 2D-Video Disdrometer," J. Atmos. Oc. Tech., Vol.25, pp. 1717-1723, 2008.

[13] D. Ohara, Y. Tajima, S. Numao, Y. Shimomura, K. Tamura, T. Yamakoshi, Takao, N. Takezawa, Y. Itou, "Development of an automatic weight measurement system for volcanic ash," Abstracts, Japan Geoscience Union Meeting (CD-ROM), V159-P025, 2009 (in Japanese).

[14] T. Takeshi, S. Tsurumoto, K. Shimokubo, S. Aso, A. Matsuoka, T. Yamakoshi, K. Tamura, D. Obara, K. Fukuda, Y. Tajima, and Y. Shimomura, "Continuous operation of Kohai-hyeto meter in Sakurajima volcano," Abstract, Japan Society Erosion Control Engineering, 2010 (in Japanese).

[15] Y. Tajima, K. Fukuda, Y. Kunimoto, E. Takahashi, K. Shimokubo, S. Aso, and M. Iguchi, "Continuous monitoring of volcanic ash falls by automatic Kohai-meters, at Sakurajima volcano," Programme and Abstracts, the Volcanological Society of Japan, 2011 (in Japanese).

[16] Y. Tajima, D. Ohara, K. Fukuda, and S. Shimomura, "Development of automatic tephrameter for monitoring of volcano," Nippon Koei Technical Forum, Vol.23, pp. 39-46, 2015.

[17] M. Maki, "Three-Dimensional Interpolated Radar Data of Volcanic Ash Clouds," Programme and Abstracts, the Volcanological Society of Japan, 2015 (Japanese).

[18] V. N. Bringi and V. Chandrasekar, "Polarimetric Doppler Weather Radar: Principles and Applications," Cambridge University Press, 2001.

[19] M. Maki, T. Maesaka, and T. Kozono, M. Nagai, R. Furukawa, S. Nakada, T. Koshida, and H. Takenaka, "Quantitative Volcanic Ash Estimation by Operational Polarimetric Weather Radara," Proc. 9th International Symposium on Tropospheric Profiling, D. Cimini, P. Di Girolamo, F. S. Marzano, and V. Rizi (Eds.), ISBN: 978-90-815839-4-7, doi:10.12898/ISTP9prc, L'Aquila, Italy, September 2012, 4pp., 2013.

[20] K. Ishihara, "Pressure sources and induced ground deformation associated with explosive eruptions at andesitic volcano: Sakurajima volcano, Japan, Magma transport and storage (Ed. M.P. Ryan)," John Wiley and Sons, pp. 335-356, 1990.

[21] M. Iguchi, "Prediction of volume of volcanic ash ejected from Showa crater of Sakurajima volcano, Japan," Annuals Disas. Prev. Res. Inst., Kyoto Univ., No.55 B, pp. 169-175, 2012 (in Japanese with English abstract).

[22] M. Iguchi, A. Yokoo, and T. Tameguri, "Intensity of Volcanic Eruptions at Showa Crater of Sakurajima Volcano," Annuals of Disas. Prev. Res. Inst., Kyoto Univ., No.53B, pp. 234-240, 2010 (in Japanese with English abstract).

[23] D. M. Harris, and WI. Rose, "Estimating particle sizes, concentrations, and total mass of ash in volcanic clouds using weather radar," J. Geophys. Res., Vol.88, pp. 10969-10983, 1983.

[24] F. S. Marzano, S. Barbieri, G. Vulpiani, and W. Rose, "Volcanic Ash Cloud Retrieval by Ground-Based Microwave Weather Radar," IEEE Trans. Geosci. Remote Sens., Vol.44, pp.3235- 3246, 2006.

[25] L. Wilson, "Explosive volcanic eruptions – II : The atmospheric trajectories of pyroclasts," Geophys. J. R. Astron. Soc., Vol.30, No.2, pp. 381-392, 1972.

[26] D. Atlas, R. S. Srivastava, and R. S. Sekhon, "Doppler radar characteristics of precipitation at vertical incidence," Rev. Geophys. Space Phys., Vol.11, pp. 1-35, 1973.

[27] T. Kozono, T. Miwa, M. Maki, T. Maesaka, D. Miki, and M. Iguchi, "PARSIVEL tephra-fall observations at Sakurajima volcano," Annuals of Disas. Prev. Inst., Kyoto Univ., No.58 B, 2015.

[28] F. S. Marzano, G. Vulpiani, and W. I. Rose, "Microphysical characterization of microwave radar reflectivity due to volcanic ash clouds," IEEE Trans. Geosci. Remote Sens., Vol.44, No.2, pp. 313-327, 2006.

[29] W. K. Brown and K. H. Wohletz, "Derivation of the Weibull distribution based on physical principles and its connection to the Rosin-Rammler and lognormal distributions," J. Appl. Phys., Vol.78, No.4, pp. 2758-2763, 1995.

[30] T. Oguchi, M. Udagawa, N. Nanba, M. Maki, and Y. Ishimine, "Measurements of Dielectric Constant of Volcanic Ash Erupted From Five Volcanoes in Japan," IEEE Trans Geosci. Remote Sensing, Vol.47, No.4, pp. 1089-1096, 2009.

[31] Kagoshima Local Meteorological Observatory, http://www.jma-net.go.jp/kagoshima/vol/data/skr_ash_vol.html, 2015.

[32] M. Maki, M. Iguchi, E. Fujita, T. Miwa, T. Maesaka, Y. Shussse, T. Kozono, T. Momotani, and A. Yamaji, "Weather Radar Observations of Sakurajima Volcanic Smoke," Annuals of Disas. Prev. Res. Inst., Kyoto Univ., No.58B, pp. 76-85, 2015 (in Japanese with English abstract).

Name:
Masayuki Maki

Affiliation:
Professor, Research and Education Center for Natural Hazards, Kagoshima University

Address:
1-21-40 Korimoto, Kagoshima 890-0065, Japan

Brief Career:
1985- Joined National Research Institute for Earth Science and Disaster Prevention
1989-1990 Visiting Scientist, the National Severe Storms Laboratory, Oklahoma, USA
1998-2000 Visiting Scientist, the Bureau of Meteorology Research Centre, Australia
2013- Kagoshima University

Selected Publications:
• M. Maki, S.-G. Park, and V. N. Bringi, 2005b, "Effect of Natural Variations in Rain Drop Size Distributions on Rain Rate Estimators of 3 cm Wavelength Polarimetric Radar," J. Meteor. Soc. Japan, Vol.83, pp. 871-893, 2005.

Academic Societies & Scientific Organizations:
• Japan Geoscience Union (JGU)
• Meteorological Society of Japan (MSJ)
• Volcanological Society of Japan (VSJ)

Name:
Masato Iguchi

Affiliation:
Disaster Prevention Research Institute, Kyoto University

Address:
1722-19 Sakurajima-Yokoyama, Kagoshima 891-1419, Japan

Brief Career:
1981- Research Associate, DPRI
1995- Associate Professor, DPRI
2012- Professor, DPRI

Selected Publications:
• Magma movement from the deep to shallow Sakurajima volcano as revealed by geophysical observations, Bull. Volcanol. Soc. Japan, Vol.58, pp. 1-18, 2013.
• Volcanic Earthquakes and Tremors in Japan, Kyoto University Press, p. 253, 2011.

Academic Societies & Scientific Organizations:
• Volcanological Society of Japan (VSJ)
• American Geophysical Union (AGU)

Name:
Takeshi Maesaka

Affiliation:
Senior Researcher, Ph.D., National Research Institute for Earth Science and Disaster Prevention (NIED)

Address:
3-1 Tennodai, Tsukuba-shi, Ibaraki 305-0006, Japan

Brief Career:
2002 Research Fellowship for Young Scientist, Japan Society for the Promotion of Science
2004 Post-Doctoral Fellow, University of Toronto
2005- National Research Institute for Earth Science and Disaster Prevention

Selected Publications:
• T. Maesaka, G. W. K. Moore, Q. Liu, and K. Tsuboki, "A Simulation of a lake effect snowstorm with a cloud resolving numerical model," Geophysical Research Letters, L20813-doi:10.1029/2006GL026638, 2006.

Academic Societies & Scientific Organizations:
• Meteorological Society of Japan (MSJ)

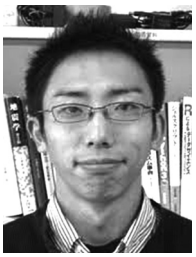

Name:
Takahiro Miwa

Affiliation:
Researcher, Ph.D., National Research Institute for Earth Science and Disaster Prevention (NIED)

Address:
3-1 Tennodai, Tsukuba, Ibaraki 305-0006, Japan

Brief Career:
2010 Postdoc, Geological survey of Japan
2011 COE Fellow, Tohoku University
2013 Postdoc, Kyushu University
2014 Researcher, National Research Institute for Earth Science and Disaster Prevention

Selected Publications:
• "Temporal variation in volcanic ash texture during a vulcanian eruption at the Sakurajima volcano, Japan," JVGR, Journal of Volcanology and Geothermal Research, Vol.260, pp. 80-89, June 2013.

Academic Societies & Scientific Organizations:
• Volcanological Society of Japan (VSJ)
• American Geophysical Union (AGU)

Name:
Toshikazu Tanada

Affiliation:
Chief Researcher, Dr., National Research Institute for Earth Science and Disaster Prevention (NIED)

Address:
3-1 Tennodai, Tsukuba-shi, Ibaraki 305-0006, Japan

Brief Career:
1987 Hot Springs Research Institute of Kanagawa Prefecture
2010 National Research Institute for Earth Science and Disaster Prevention (NIED)

Selected Publications:
• "Seismicity in the northeast area of Izu Peninsula, Japan, comparing with three dimensional velocity structure and with temperature distribution of geothermal water," Tectonophysics, pp. 449-460, 306 3/4, 1999.

Academic Societies & Scientific Organizations:
• Volcanological Society of Japan (VSJ)
• Seismological Society of Japan (SSJ)

Name:
Tomofumi Kozono

Affiliation:
Assistant Professor, Ph.D., Department of Geophysics, Graduate School of Science, Tohoku University

Address:
6-3 Aramaki-Aza-Aoba, Aoba-ku, Sendai 980-8578, Japan

Brief Career:
2007-2009 Project Researcher, Earthquake Research Institute, University of Tokyo
2009-2013 Researcher, National Research Institute for Earth Science and Disaster Prevention
2013- Tohoku University

Selected Publications:
• T. Kozono, H. Ueda, T. Shimbori, and K. Fukui, "Correlation between magma chamber deflation and eruption cloud height during the 2011 Shinmoe-dake eruptions," Earth Planets Space, Vol.66, 139, Oct., 2014.
• T. Kozono, H. Ueda, T. Ozawa, T. Koyaguchi, E. Fujita, A. Tomiya, and Suzuki, Y. J., "Magma discharge variations during the 2011 eruptions of Shinmoe-dake volcano, Japan, revealed by geodetic and satellite observations," Bull. Volcanol., Vol.75, 695, Feb., 2013.
• T. Kozono and T. Koyaguchi, "Effects of gas escape and crystallization on the complexity of conduit flow dynamics during lava dome eruptions," J. Geophys. Res., Vol.117, Aug., 2012.

Academic Societies & Scientific Organizations:
• Volcanological Society of Japan (VSJ)
• Japan Geoscience Union (JpGU)
• American Geophysical Union (AGU)

Name:
Tatsuya Momotani

Affiliation:
Senior Engineer, Japan Weather Association

Address:
Sunshine60 Bldg. 55F, 3-1-1 Higashi-Ikebukuro, Toshima-ku, Tokyo 170-6055, Japan

Brief Career:
2001 Joined Japan Weather Association

Name:
Akihiko Yamaji

Affiliation:
General Manager, Japan Weather Association

Address:
Sunshine60 Bldg. 55F, 3-1-1 Higashi-Ikebukuro, Toshima-ku, Tokyo 170-6055, Japan

Brief Career:
1986 Joined Japan Weather Association

Academic Societies & Scientific Organizations:
• Japan Society of Civil Engineers (JSCE)
• Japan Society of Hydrology and Water Resources (JSHWR)

Name:
Ikuya Kakimoto

Affiliation:
Chief Engineer, Environment Monitoring and Traffic Control System Section, Mitsubishi Electric Corporation

Address:
8-1-1 Tsukaguchi-Honmachi, Amagasaki City, Hyogo 661-8661, Japan

Brief Career:
1987- Mitsui Mining & Semelting Corp.
1989- Mitsubishi Electric Corporation